ACS APPLIED MATERIALS & INTERFACES

Letter

www.acsami.org

Use of Ultrafast Time-Resolved Spectroscopy to Demonstrate the Effect of Annealing on the Performance of P3HT:PCBM Solar Cells

Yu-Ting Wang,[†] Mei-Hsin Chen,*[,‡] Chao-Ting Lin,[†] Jian-Jhih Fang,[‡] Che-Jui Chang,[‡] Chih-Wei Luo,*[,†,§] Atsushi Yabushita,[†] Kaung-Hsiung Wu,[†] and Takayoshi Kobayashi[†,⊥,#]

[†]Department of Electrophysics, National Chiao Tung University, Hsinchu 30010, Taiwan

[‡]Department of Optoelectronic Engineering, National Dong Hwa University, Hualien 974, Taiwan

[§]Taiwan Consortium of Emergent Crystalline Materials, Ministry of Science and Technology, Taipei 10601, Taiwan

[⊥]Advanced Ultrafast Laser Research Center and Department of Engineering Science, The University of Electro-Communications, Chofu, Tokyo 182-8585, Japan

[#]CREST, JST, 5 Sanbancho, Chiyoda-Ku, Tokyo 102-0075, Japan

Supporting Information

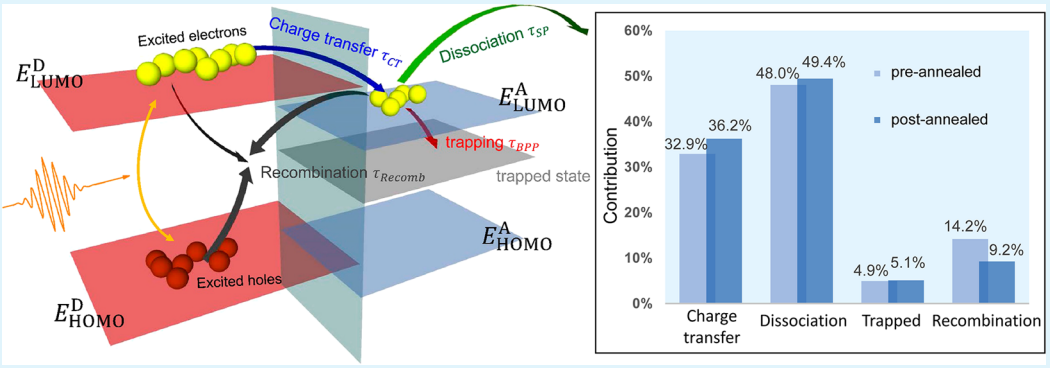

ABSTRACT: The organic solar cells of heterojunction system, ITO/PEDOT:PSS/P3HT:PCBM/Al, with a thermal annealing after deposition of Al exhibit better performance than those with an annealing process before deposition of Al. In this study, ultrafast time-resolved spectroscopy is employed to reveal the underlying mechanism of annealing effects on the performance of P3HT:PCBM solar cell devices. The analyses of all decomposed relaxation processes show that the postannealed devices exhibit an increase in charge transfer, in the number of separated polarons and a reduction in the amount of recombination between excited carriers. Moreover, the longer lifetime for the excited carriers in postannealed devices indicates it is more likely to be dissociated into photocarriers and result in a larger value for photocurrent, which demonstrates the physical mechanism for increased device performance.

KEYWORDS: *organic solar cells, ultrafast dynamics, annealing effect*

In the past couple of decades, organic solar cells have evolved as a cost-effective alternative to silicon-based solar cells. Organic solar cells can be made into devices that are lighter in weight and more flexible than photovoltaics that use traditional inorganic semiconductors.[1,2] For standard bulk heterojunction systems, poly(3-hexylthiophene) (P3HT) as the electron donor and [6,6]-pheny1-C61-butyric acid methyl ester (PCBM) as the electron acceptor are frequently mixed to create a composite material, that has been demonstrated to give effective device performance.[3] To optimize the efficiency of these composite materials, the correlation between the fabrication processes and device performance, as well as the basic operation mechanisms, requires detailed study. It is known that the devices that use the simple structure, ITO/PEDOT:PSS/P3HT:PCBM/Al, with an annealing process after deposition of Al (post annealing), have better performance than those with an annealing process before the deposition of Al (preannealing). Recently, the variation of surface morphology and vertical distribution of P3HT:PCBM blends after an annealing process has been studied using atomic force microscopy,[4] photoemission spectroscopy,[5,6] transmission electron microscopy,[7,8] and grazing-incidence wide-angle X-ray scattering[9,10] in order to determine the reasons for the high performance. However, the carrier dynamics directly correlate to the efficiency of charge transport in solar cell devices remain unexplained.

Ultrafast optical pump−probe spectroscopy has proven to be a powerful tool for the study of the relaxation processes

Received: November 18, 2014
Accepted: February 18, 2015
Published: February 18, 2015

DOI: 10.1021/am508091u
ACS Appl. Mater. Interfaces 2015, 7, 4457−4462

through electron−electron interaction,[11] electron−phonon interaction,[12−14] and electron−spin interaction[15,16] in various materials. To understand the underlying mechanisms in materials, the interactions between the order parameters must be derived first. By observing the difference in the characteristic time scales and behavior for the various degrees of freedom in complex structures or composite materials, ultrafast spectroscopy can be used to determine the individual dynamics and the relationship between different order parameters. Therefore, some transient spectroscopic studies in organic photovoltaic materials have shed light on improving the device performance.[17−19] Pensack and Asbury directly observed the formation and dissociation of charge-transfer states of the heterojunction systems in which the delocalized electron and hole wave functions exhibit efficient dissociation rate by ultrafast solvatochromism.[20] In addition, the enhancement of free charge generation rate was measured in annealed regioregular P3HT:PCBM blends.[21] It was also found that the exciton diffusion, charge transfer, and charge dissociation are strongly dependent on blend structures.[22] On the basis of the above studies, the transient spectroscopy can be further used to reveal the underlying mechanism for the different performance of pre/post-annealed devices.

In this study, the ultrafast carrier dynamics (charge generation and the recombination) in pre/post-annealed P3HT:PCBM devices was systematically investigated by monitoring the changes of transient absorbance in visible region. The absorbance changes as a function of wavelength and time were measured to reveal the correlation between the carrier dynamics and the photovoltaic properties. By analyzing the carrier relaxation dynamics, a model for energy transfer in pre/post-annealed devices were established.

Figure 1 shows the current density−voltage (J−V) characteristics for a device with the structure of ITO/PEDOT:PSS/P3HT:PCBM/Al and different thermal annealing processes. The devices were fabricated using preannealing or postannealing processes. To fabricate the devices using the preannealing processes, the as-cast P3HT:PCBM was thermally annealed at 190 °C for 10 min, prior to deposition of the Al cathode. For the fabrication of the devices using a postannealing process, the Al cathode was deposited on the as-cast P3HT:PCBM and this was then annealed at 190 °C for 10 min. The device performance and characteristics are further detailed in the inset of Figure 1. As expected, the device that is fabricated using a preannealing process exhibits poor characteristics and its power conversion efficiency is only 1.63%. The other device with a postannealing process demonstrates better device performance and its power conversion efficiency is 2.88%. In terms of device performance, both open circuit voltage (V_{OC}) and short circuit current (J_{SC}) are improved by the postannealing process. The device performance in this study is similar to that of the devices with the same structure (ITO/PEDOT:PSS/P3HT:PCBM/Al) reported previously.[10,23,24]

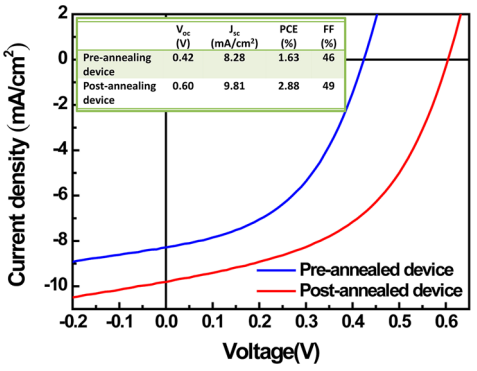

	V_{oc} (V)	J_{sc} (mA/cm²)	PCE (%)	FF (%)
Pre-annealing device	0.42	8.28	1.63	46
Post-annealing device	0.60	9.81	2.88	49

Figure 1. Current density−voltage (J−V) characteristics for the solar cells of ITO/PEDOT:PSS/P3HT:PCBM/Al with pre- and post-annealing processes. The inset table shows the characteristics of the device performance.

The devices produced by a postannealing process have been demonstrated to possess higher performance because of the changes in surface morphology and the vertical distribution of the P3HT:PCBM blends during annealing, as mentioned in previous reports.[4,5,9] The basic mechanism for charge transport is definitely important in regulating the device performance. To understand this hidden mechanism, the correlations between the carrier dynamics and the device performance for the pre/post-annealed devices must be determined. Before carried out any time- and photon energy-resolved pump−probe spectroscopy, the fundamental optical properties of P3HT:PCBM devices have to be examined. The stationary absorbance spectra for the pre- and postannealed devices in the visible range are shown in Figure 2. The absorbance increases rapidly at photon energies greater than ∼1.9 eV, which demonstrates that the polymer has a wide absorption band.[25] Both spectra for the pre- and postannealed devices show a $\pi - \pi^*$ transition of P3HT at 2.05 and 2.23 eV.[26,27]

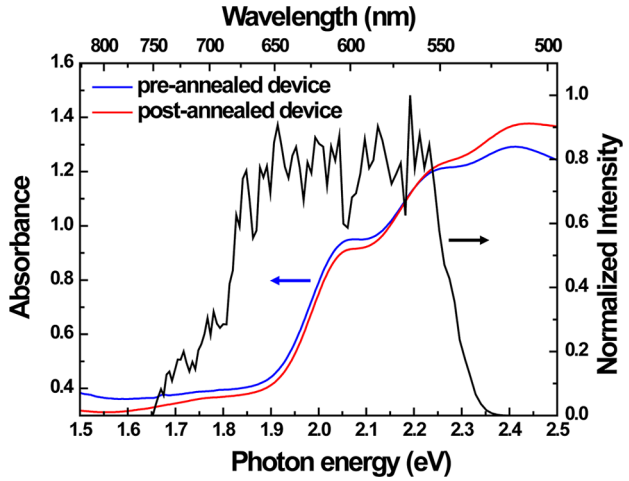

Figure 2. Stationary absorption spectra for P3HT:PCBM devices with postannealing (red) and preannealing (blue) processes. The laser spectrum of the light source used in this study is shown by black line.

Figures 3a, c show the two-dimensional plots for the time- and photon energy-resolved transient difference absorbance spectra, $\Delta A(\omega,t)$, of the devices with pre- and postannealing processes using the pump−probe technique. The ΔA spectrum is positive at photon energies of less than ∼1.98 eV, which is attributable to the induced absorption for the transitions from the first excited state to higher states. The negative ΔA at photon energies greater than ∼1.98 eV is attributed to the stimulated emission from the excited state and photobleaching due to ground state depletion. The two peaks at 2.05 and 2.23 eV represent the π−π^* transition in P3HT. Figure 4 further shows the relaxation processes of samples, which are excited by pump pulses with a photon energy of >1.9 eV (the absorption gap energy).[17,18] In the composite samples, it is estimated that

DOI: 10.1021/am508091u
ACS Appl. Mater. Interfaces 2015, 7, 4457−4462

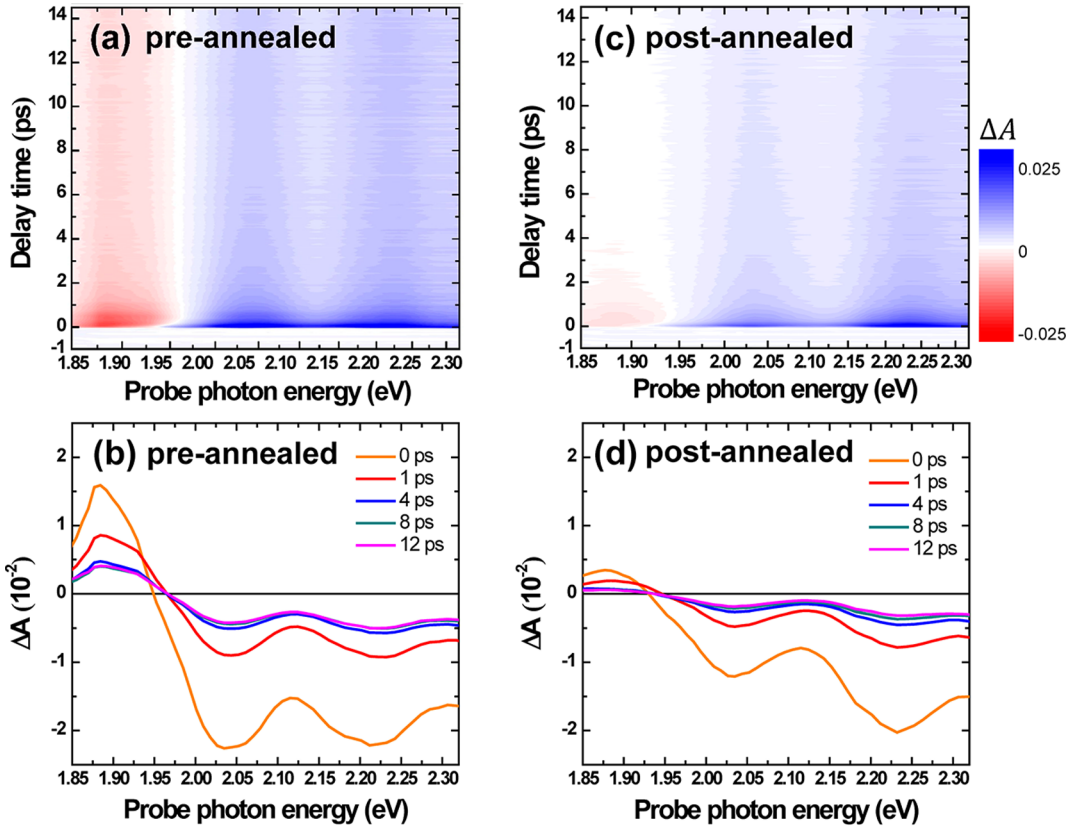

Figure 3. Two-dimensional plot of transient difference absorption $\Delta A(\omega,t)$ and $\Delta A(\omega)$ spectra at various time delays for (a, b) preannealed and (c, d) postannealed P3HT:PCBM devices.

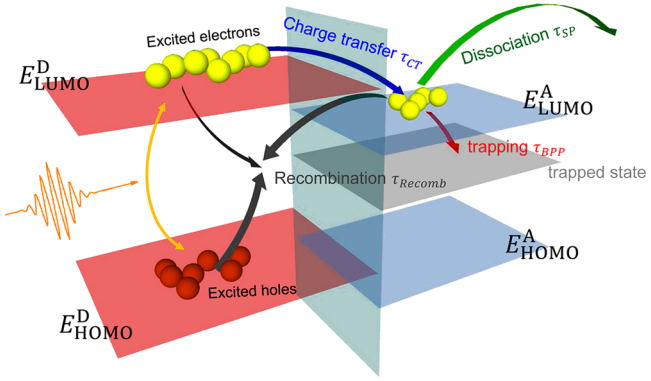

Figure 4. A schematic representation of ultrafast carrier dynamics after photoexcitation. E^{D}_{LUMO}: the lowest unoccupied molecular orbital of the electron donor. E^{D}_{LUMO}: the highest occupied molecular orbital of the electron donor. E^{A}_{LUMO}: the lowest unoccupied molecular orbital of the electron acceptor. E^{A}_{LUMO}: the highest occupied molecular orbital of the electron acceptor. In this study, the electron donor and the electron acceptor are P3HT and PCBM, respectively. τ is the time constant for the relaxation processes.

more than 60% of the incident photons are absorbed by the polymer.[28] Therefore, the sample excited by the pump pulses generates the excited electron and hole pairs, primarily in P3HT molecules. The excited electrons at the lowest unoccupied molecular orbital (LUMO) of P3HT transfer to the LUMO of PCBM and then the holes remain in the P3HT to form a bounded polaron pair (BPP) with the excited electrons. The time constant for this interfacial charge transfer is measured as ~90 fs.[18,19] The generated BPP then relaxes to the ground state, via the parallel processes of "dissociating into separated polarons", "trapping by defect states", and "recombination." The time constants for dissociating into the separated polarons and defect trapping are reported to be ~0.95 ps and ~2.8 ps,[18] respectively.

According to above scenario, the real time traces for $\Delta A(\omega,t)$ are expressed by the following equation.

$$\Delta A(t) = A_{CT}e^{-t/\tau_{CT}} + A_{SP}(-e^{-t/\tau_{CT}} + e^{-t/\tau_{SP}}) + A_{trap}(-e^{-t/\tau_{CT}} + e^{-t/\tau_{trap}}) + A_{Recomb} \quad (1)$$

where the suffixes CT, SP, trap, and Recomb, correspond to charge transfer, separated polarons (dissociated BPP), trapped BPP, and carrier recombination, respectively. The fitting results are shown in Figure 5a–f. The time constant for carrier recombination is beyond the measurement range in this study. For the device fabricated by a postannealing process, the time constants, τ_{CT}, τ_{SP}, and τ_{trap}, are ~0.13, ~0.68, and ~8.48 ps, respectively. For the preannealed device, the time constants, τ_{CT}, $\tau_{SP,}$ and τ_{trap}, are ~0.13, ~0.54, and ~2.60 ps, respectively. The relaxation processes for BPP, especially for trapping by defect states (τ_{trap}), apparently have a longer lifetime in the device with a postannealing process. This implies that the excited carriers in the E^{A}_{LUMO} state have a longer lifetime and so are more likely to be dissociated into photocarriers that further produce a photocurrent. Accordingly, this longer lifetime of the excited carriers in the device with a postannealing process may explain the increase in the J_{SC} value. However, in reality there are serval relaxation channels for the excited carriers in the E^{A}_{LUMO} state, such as dissociating into separated polarons, trapping by defect states and recombination. In the case where

DOI: 10.1021/am508091u
ACS Appl. Mater. Interfaces 2015, 7, 4457–4462

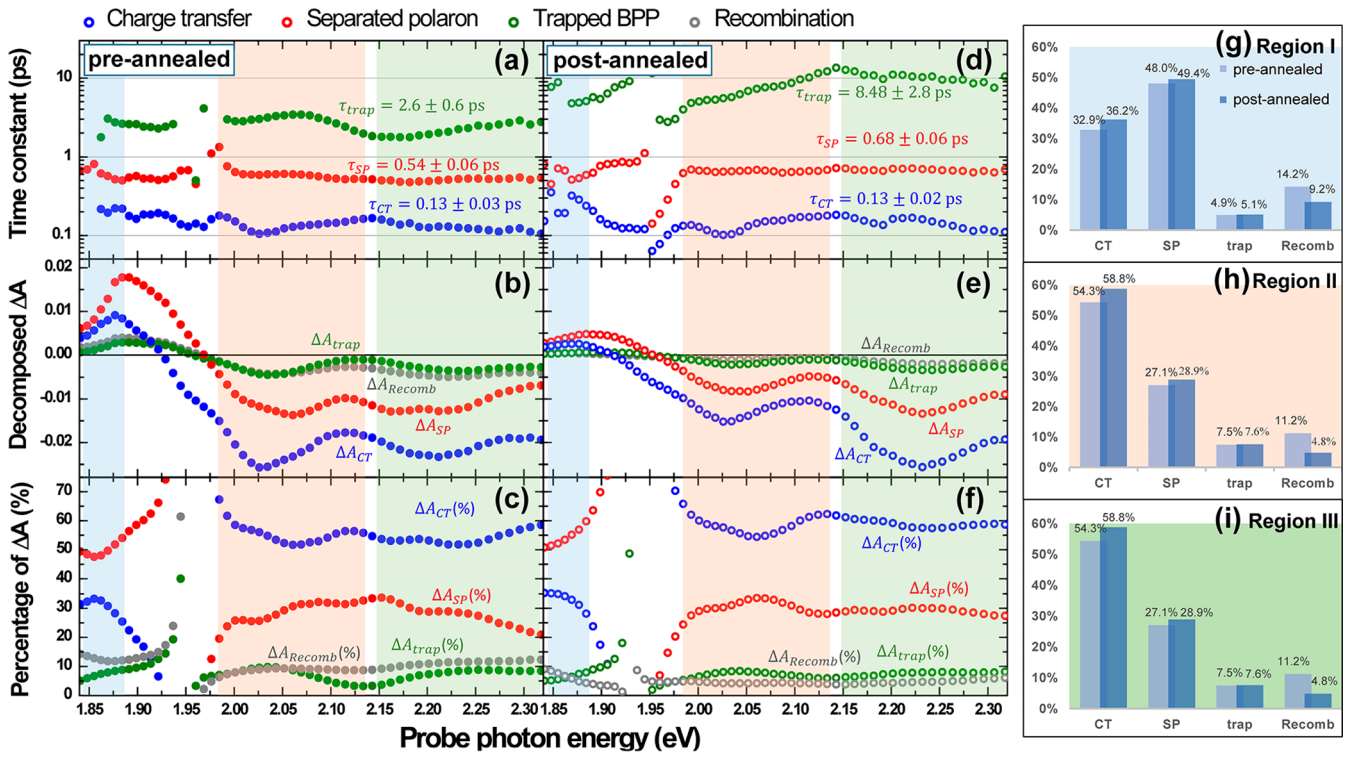

Figure 5. Exponential fitting results, using eq 1 (see text), for (a, b) preannealed devices and (d, e) postannealed devices. The blue, red, green, and gray traces respectively represent charge transfer, separated polarons, trapped BPP and recombination. (c, f) Percentage for the decomposed relaxation processes in b and e. (g–i) Average percentage for the decomposed relaxation processes in the three different regions, at ~1.88, ~2.05, and ~2.23 eV, respectively.

most excited carriers in the E^{A}_{LUMO} state are trapped by defect states or recombine with opposite charges, without contribution to the photocurrent, then these excited carriers certainly do not produce an increase in the value of $J_{SC,}$ even though they have longer lifetime in the E^{A}_{LUMO} state. Consequently, it is necessary to determine how many excited carriers in the E^{A}_{LUMO} state relax through each channel, which is still unresolved.

It is worth emphasizing that pump–probe spectroscopy with high time- and photon energy-resolution can be further used to show the total amount of all relaxation processes in the E^{A}_{LUMO} state (see Figure 4), which is the key to understanding any improvement in device performance. The percentage of carriers relaxed through every channel is calculated using the coefficients, A_{CT}, A_{SP}, A_{trap}, and A_{Recomb}. Figures 5g–i show the percentage of decomposed components in the three different regions. Region I shows the induced absorption at ~1.88 eV. Regions II and III contain the peaks for stimulated emission and photobleaching, at ~2.05 and ~2.23 eV, respectively. In these three regions, the percentage of charge transfer increases by ~3.5% for the postannealed devices. This demonstrates that the interfacial charge transfer from an electron donor (P3HT) to an electron acceptor (PCBM) in the devices with a postannealing process is more efficient than that in the preannealed devices. There are ~1.6% more separated polarons in the postannealed devices than that in the preannealed devices, but there is ~5.2% less recombination in the postannealed devices. Consequently, more charges transfer from an electron donor (P3HT) to an electron acceptor (PCBM). More separated polarons and less recombination mean that there are more effective free carriers, which produces a larger short circuit current (J_{SC}) in the postannealed devices, as shown in Figure 1.

In P3HT:PCBM blend films, moreover, ultrafast dynamics studies showed that the photovoltaic efficiency can be significantly affected by the blend morphology, rather than excess energy.[21] Further compare with the unannealed P3HT:PCBM blend films, the charge transfer, charge dissociation and charge collection in the annealed P3HT:PCBM blend films are strongly dependent on the blend structue.[21,22] Therefore, we argue that the structural morphology in our devices would be influenced by the Al layer during the annealing process, which leads to the difference in carrier dynamics and device performance. These results are consistent with previous studies on surface morphology and the vertical distribution of P3HT:PCBM blends during annealing.[4−6,8,10] It has been reported that the presence of an Al layer on top of the P3HT:PCBM layer reduces the crystallization of P3HT during thermal annealing, which results in a surface segregated PCBM-rich layer at the Al interface and further increases the effective built-in field. The desirable hole-blocking layers, i.e., the surface segregation of PCBM at the Al interface induced by a postannealing process, increase the charge transfer and the number of separated polarons, but reduce the amount of recombination between electrons and holes, which is the source of the significant performance improvement in the postannealed devices.

In conclusion, ultrafast time-resolved spectroscopy clearly shows the effect of annealing processes on the performance of P3HT:PCBM solar cells. The longer lifetime of the excited carriers in the E^{A}_{LUMO} state of the postannealed devices results in a larger value of J_{SC}. The analyses of all decomposed relaxation processes show that there is an increase in charge transfer, in the number of separated polarons and a reduction in the amount of recombination between excited carriers, which is one

DOI: 10.1021/am508091u
ACS Appl. Mater. Interfaces 2015, 7, 4457–4462

of the physical mechanism responsible for increasing the performance by a postannealing process. These findings are consistent with the observations on the annealing-dependent surface morphology and the vertical distribution of P3HT:PCBM blends. Finally, this study provides key information for the design of high-performance solar cells.

■ ASSOCIATED CONTENT

Supporting Information

The authors declare no competing financial interest. This material is available free of charge via the Internet at http://pubs.acs.org.

■ AUTHOR INFORMATION

Corresponding Authors

*E-mail: meihsinchen@mail.ndhu.edu.tw.

*E-mail: cwluo@mail.nctu.edu.tw.

Notes

The authors declare no competing financial interest.

■ ACKNOWLEDGMENTS

This project is financially sponsored by the Ministry of Science and Technology, Taiwan, Republic of China (Grants 101-2112-M-009-016-MY2, 103-2923-M-009-001-MY3, 103-2628-M-009-002-MY3, 103-2119-M-009-004-MY3, and 103-2112-M-259-007-MY3.) and the Ministry of Education (MOE-ATU plan at National Chiao Tung University).

■ REFERENCES

(1) Stubhan, T.; Salinas, M.; Ebel, A.; Krebs, F. C.; Hirsch, A.; Halik, M.; Brabec, C. J. Increasing the Fill Factor of Inverted P3HT:PCBM Solar Cells Through Surface Modification of Al-Doped ZnO via Phosphonic Acid-Anchored C60 SAMs. *Adv. Energy Mater.* **2012**, *2*, 532−535.

(2) Krebs, F. C.; Søndergaard, R.; Jørgensen, M. Printed Metal Back Electrodes for R2R Fabricated Polymer Solar Cells Studied Using the LBIC Technique. *Sol. Energy Mater. Sol. Cells* **2011**, *95*, 1348−1353.

(3) Dennler, G.; Scharber, M. C.; Brabec, C. J. Polymer-Fullerene Bulk-Heterojunction Solar Cells. *Adv. Mater.* **2009**, *21*, 1323−1338.

(4) Fang, J. J.; Tsai, H. W.; Ni, I. C.; Tzeng, S. D.; Der Chen, M. H. The Formation of Interfacial Wrinkles at the Metal Contacts on Organic Thin Films. *Thin Solid Films* **2014**, *556*, 294−299.

(5) Tseng, W. H.; Lo, H.; Chang, J. K.; Liu, I. H.; Chen, M. H.; Wu, C. I. Metal-Induced Molecular Diffusion in [6,6]-Phenyl-C61-Butyric Acid Methyl Ester poly(3-Hexylthiophene) Based Bulk-Heterojunction Solar Cells. *Appl. Phys. Lett.* **2013**, *103*, 183506.

(6) Orimo, A.; Masuda, K.; Honda, S.; Benten, H.; Ito, S.; Ohkita, H.; Tsuji, H. Surface Segregation at the Aluminum Interface of Poly (3-Hexylthiophene)/Fullerene Solar Cells. *Appl. Phys. Lett.* **2010**, *96*, 043305.

(7) Park, J. H.; Kim, J. S.; Lee, J. H.; Lee, W. H.; Cho, K. Effect of Annealing Solvent Solubility on the Performance of Poly(3-hexylthiophene)/Methanofullerene Solar Cells. *J. Phys. Chem. C* **2009**, *113*, 17579−17584.

(8) Ebadian, S.; Gholamkhass, B.; Shambayati, S.; Holdcroft, S.; Servati, P. Effects of Annealing and Degradation on Regioregular Polythiophene-Based Bulk Heterojunction Organic Photovoltaic Devices. *Sol. Energy Mater. Sol. Cells* **2010**, *94*, 2258−2264.

(9) Treat, N. D.; Brady, M. A.; Smith, G.; Toney, M. F.; Kramer, E. J.; Hawker, C. J.; Chabinyc, M. L. Interdiffusion of PCBM and P3HT Reveals Miscibility in a Photovoltaically Active Blend. *Adv. Energy Mater.* **2011**, *1*, 82−89.

(10) Kim, H. J.; Park, J. H.; Lee, H. H.; Lee, D. R.; Kim, J.-J. The Effect of Al Electrodes on the Nanostructure of Poly(3-Hexylthiophene): Fullerene Solar Cell Blends during Thermal Annealing. *Org. Electron.* **2009**, *10*, 1505−1510.

(11) Eichberger, M.; Schäfer, H.; Krumova, M.; Beyer, M.; Demsar, J.; Berger, H.; Moriena, G.; Sciaini, G.; Miller, R. J. D. Snapshots of Cooperative Atomic Motions in the Optical Suppression of Charge Density Waves. *Nature* **2010**, *468*, 799−802.

(12) Luo, C. W.; Wu, I. H.; Cheng, P. C.; Lin, J.-Y.; Wu, K. H.; Uen, T. M.; Juang, J. Y.; Kobayashi, T.; Chareev, D. A.; Volkova, O. S.; et al. Quasiparticle Dynamics and Phonon Softening in FeSe Superconductors. *Phys. Rev. Lett.* **2012**, *108*, 257006.

(13) Luo, C. W.; Wu, I. H.; Cheng, P. C.; Lin, J.-Y.; Wu, K. H.; Uen, T. M.; Juang, J. Y.; Kobayashi, T.; Wen, Y. C.; Huang, T. W.; et al. Ultrafast Dynamics and Phonon Softening in $Fe_{1+y}Se_{1-x}Te_x$ Single Crystals. *New J. Phys.* **2012**, *14*, 103053.

(14) Luo, C. W.; Wang, H. J.; Ku, S. A.; Chen, H.-J.; Yeh, T. T.; Lin, J.-Y.; Wu, K. H.; Juang, J. Y.; Young, B. L.; Kobayashi, T.; et al. Snapshots of Dirac Fermions near the Dirac Point in Topological Insulators. *Nano Lett.* **2013**, *13*, 5797−5802.

(15) Shih, H. C.; Lin, T. H.; Luo, C. W.; Lin, J.-Y.; Uen, T. M.; Juang, J. Y.; Wu, K. H.; Lee, J. M.; Chen, J. M.; Kobayashi, T. Magnetization Dynamics and the Mn^{3+} d-d Excitation of Hexagonal $HoMnO_3$ Single Crystals Using Wavelength-Tunable Time-Resolved Femtosecond Spectroscopy. *Phys. Rev. B* **2009**, *80*, 024427.

(16) Shih, H. C.; Chen, L. Y.; Luo, C. W.; Wu, K. H.; Lin, J.-Y.; Juang, J. Y.; Uen, T. M.; Lee, J. M.; Chen, J. M.; Kobayashi, T. Ultrafast Thermoelastic Dynamics of $HoMnO_3$ Single Crystals Derived from Femtosecond Optical Pump−probe Spectroscopy. *New J. Phys.* **2011**, *13*, 053003.

(17) Ai, X.; Beard, M. C.; Knutsen, K. P.; Shaheen, S. E.; Rumbles, G.; Ellingson, R. J. Photoinduced Charge Carrier Generation in a Poly(3-Hexylthiophene) and Methanofullerene Bulk Heterojunction Investigated by Time-Resolved Terahertz Spectroscopy. *J. Phys. Chem. B* **2006**, *110*, 25462−25471.

(18) Lee, Y. H.; Yabushita, A.; Hsu, C. S.; Yang, S. H.; Iwakura, I.; Luo, C. W.; Wu, K. H.; Kobayashi, T. Ultrafast Relaxation Dynamics of Photoexcitations in Poly(3-Hexylthiophene) for the Determination of the Defect Concentration. *Chem. Phys. Lett.* **2010**, *498*, 71−76.

(19) Brabec, C.; Zerza, G.; Cerullo, G.; De Silvestri, S.; Luzzati, S.; Hummelen, J. C.; Sariciftci, S. Tracing Photoinduced Electron Transfer Process in Conjugated Polymer/Fullerene Bulk Heterojunctions in Real Time. *Chem. Phys. Lett.* **2001**, *340*, 232−236.

(20) Pensack, R. D.; Asbury, J. B. Ultrafast Probes of Charge Transfer States in Organic Photovoltaic Materials. *Chem. Phys. Lett.* **2011**, *515*, 197−205.

(21) Howard, I. A.; Mauer, R.; Meister, M.; Laquai, F. Effect of Morphology on Ultrafast Free Carrier Generation in Polythiophene:-Fullerene Organic Solar Cells. *J. Am. Chem. Soc.* **2010**, *132*, 14866−14876.

(22) Guo, J.; Ohkita, H.; Benten, H.; Ito, S. Charge Generation and Recombination Dynamics in Poly(3-Hexylthiophene)/Fullerene Blend Films with Different Regioregularities and Morphologies. *J. Am. Chem. Soc.* **2010**, *132*, 6154−6164.

(23) Kim, Y.; Choulis, S. A.; Nelson, J.; Bradley, D. D. C.; Cook, S.; Durrant, J. R. Device Annealing Effect in Organic Solar Cells with Blends of Regioregular Poly(3-Hexylthiophene) and Soluble Fullerene. *Appl. Phys. Lett.* **2005**, *86*, 063502.

(24) Wang, W.; Wu, H.; Yang, C.; Luo, C.; Zhang, Y.; Chen, J.; Cao, Y. High-Efficiency Polymer Photovoltaic Devices from Regioregular-Poly(3-Hexylthiophene-2,5-Diyl) and [6,6]-Phenyl-C_{61}-Butyric Acid Methyl Ester Processed with Oleic Acid Surfactant. *Appl. Phys. Lett.* **2007**, *90*, 183512.

(25) Winder, C.; Sariciftci, N. S. Low Bandgap Polymers for Photon Harvesting in Bulk Heterojunction Solar Cells. *J. Mater. Chem.* **2004**, *14*, 1077−1086.

(26) Shrotriya, V.; Ouyang, J.; Tseng, R. J.; Li, G.; Yang, Y. Absorption Spectra Modification in Poly(3-Hexylthiophene): Methanofullerene Blend Thin Films. *Chem. Phys. Lett.* **2005**, *411*, 138−143.

(27) Zhao, Y.; Xie, Z.; Qu, Y.; Geng, Y.; Wang, L. Solvent-Vapor Treatment Induced Performance Enhancement of Poly(3-Hexylthiophene): Methanofullerene Bulk-Heterojunction Photovoltaic Cells. *Appl. Phys. Lett.* **2007**, *90*, 043504.

DOI: 10.1021/am508091u
ACS Appl. Mater. Interfaces 2015, 7, 4457−4462

(28) Savenije, T. J.; Kroeze, J. E.; Wienk, M. M.; Kroon, J. M.; Warman, J. W. Mobility and Decay Kinetics of Charge Carriers in Photoexcited PCBM/PPV Blends. *Phys. Rev. B* **2004**, *69*, 155205.

DOI: 10.1021/am508091u
ACS Appl. Mater. Interfaces 2015, 7, 4457−4462